

1 Selective Reduction of CO₂ to CH₄ by Tandem Hydrosilylation with 2 Mixed Al/B Catalysts

3 Jiawei Chen,[†] Laura Falivene,^{*,‡} Lucia Caporaso,[§] Luigi Cavallo,[‡] and Eugene Y.-X. Chen^{*,†}

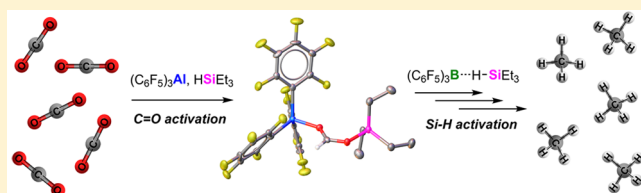
4 [†]Department of Chemistry, Colorado State University, Fort Collins, Colorado 80523-1872, United States

5 [‡]Physical Sciences and Engineering Division, Kaust Catalysis Center (KCC), King Abdullah University of Science and Technology
6 (KAUST), Thuwal 23955-6900, Saudi Arabia

7 [§]Dipartimento di Chimica e Biologia, Università di Salerno, Via Papa Paolo Giovanni II, I-84084 Fisciano, Italy

8 **S** Supporting Information

9 **ABSTRACT:** This contribution reports the first example of
10 highly selective reduction of CO₂ into CH₄ via tandem
11 hydrosilylation with mixed main-group organo-Lewis acid
12 (LA) catalysts [Al(C₆F₅)₃ + B(C₆F₅)₃] {[Al] + [B]}. As shown
13 by this comprehensive experimental and computational study,
14 in this unique tandem catalytic process, [Al] effectively
15 mediates the first step of the overall reduction cycle, namely
16 the fixation of CO₂ into HCOOSiEt₃ (**1**) via the LA-mediated
17 C=O activation, while [B] is incapable of promoting the same transformation. On the other hand, [B] is shown to be an
18 excellent catalyst for the subsequent reduction steps 2–4, namely the hydrosilylation of the more basic intermediates [I to
19 H₂C(OSiEt₃)₂ (**2**) to H₃COSiEt₃ (**3**) and finally to CH₄] through the frustrated Lewis pair (FLP)-type Si–H activation. Hence,
20 with the required combination of [Al] and [B], a highly selective hydrosilylative reduction of CO₂ system has been developed,
21 achieving high CH₄ production yield up to 94%. The remarkably different catalytic behaviors between [Al] and [B] are attributed
22 to the higher overall Lewis acidity of [Al] derived from two conflicting factors (electronic and steric effects), which renders the
23 higher tendency of [Al] to form stable [Al]–substrate (intermediate) adducts with CO₂ as well as subsequent intermediates **1**, **2**,
24 and **3**. Overall, the roles of [Al] and [B] are not only complementary but also synergistic in the total reduction of CO₂, which
25 render both [Al]-mediated first reduction step and [B]-mediated subsequent steps catalytic.



26 ■ INTRODUCTION

27 Achieving efficient direct and catalytic reduction of CO₂ into
28 CH₄ will have significant impact on addressing two currently
29 biggest issues facing humanity: global warming largely due to
30 the rising level of the greenhouse gas CO₂ and increasing
31 demand on clean energy such as solar energy and natural gas
32 CH₄. Although CO₂ is considered to be an ideal renewable C₁
33 feedstock for chemicals, materials, and fuels as it is renewable,
34 abundant, nonflammable, and inexpensive,¹ it is a highly stable,
35 inert molecule, so it has been a challenge to develop
36 technologically feasible and economically competitive methods
37 to convert CO₂ into fuels, especially high-energy density,
38 deoxygenated fuels such as methane.² Catalytic hydrosilylation
39 of CO₂, although with silanes as an expensive hydrogen source,
40 is a thermodynamically favored process with formation of
41 stronger Si–O bonds,³ when compared to the catalytic
42 hydrogenation of CO₂.⁴ Currently, transition-metal (TM)
43 catalysts based on metals such as Ru,⁵ Co,⁶ Rh,⁷ Ir,⁸ Ni,⁹
44 Cu,¹⁰ and main-group Zn¹¹ have been utilized but achieved
45 limited success in the catalytic hydrosilylation of CO₂ to lower
46 oxidation state species with low selectivity for methane
47 formation.²

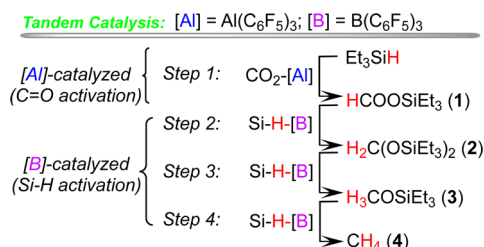
48 An emerging approach to enhancing catalytic performance of
49 the CO₂ hydrosilylation systems is to couple the strong organo-
50 Lewis acid B(C₆F₅)₃,¹² which, when used alone, is incapable of

reducing CO₂,¹³ with TM complexes of Zr,¹³ Pt, Pd,¹⁴ Re,¹⁵
51 and Sc¹⁶ for fixation of CO₂ (by TM complexes) and
52 subsequent reduction of the more basic formate, aldehyde,
53 and methanol to CH₄ (by the borane). More recently, there is
54 emerging interest in the development of TM-free catalysis
55 spotlighted by frustrated Lewis pairs (FLPs).¹⁷ O'Hare et al.
56 reported CO₂ can be hydrogenated to CH₃OH with the 2,2,6,6-
57 tetramethylpiperidine (TMP)/B(C₆F₅)₃ FLP system.¹⁸ Alter-
58 natively, Stephan¹⁹ et al. demonstrated the combination of
59 PMes₃/AlX₃ (Mes = mesityl, X = Cl, Br) effects the reduction
60 of CO₂ to CH₃OH with H₃NBH₃ as a hydrogen source.
61 However, both of these transformations require a stoichio-
62 metric amount of the FLP reagents. In this regard, Fontaine et al.
63 discovered an ambiphilic Lewis pair system with a less Lewis
64 acidic catecholboronyl unit which can promote the release of the
65 reduced products from the catalyst and thus render the
66 hydroboration of CO₂ catalytic.²⁰ Ever since, major exper-
67 imental and computational efforts have been directed to the
68 study of the CO₂ reduction utilizing the FLP chemistry.^{21,22} On
69 the other hand, only a few examples of catalytic hydrosilylation
70 of CO₂ have surfaced in the literature by utilizing either the
71 separate reactivity of Lewis acid (LA)/Lewis base (LB) or the

Received: February 9, 2016

73 combination of them. For instance, Ying et al. reported NHC-
 74 catalyzed CO₂ reduction with H₂SiPh₂,²³ while Piers utilized
 75 B(C₆F₅)₃ (in excess) and TMP for deoxygenative hydro-
 76 silylation of CO₂.²⁴ Müller et al. demonstrated that silyl cations
 77 are effective in promoting conversion of CO₂ into benzoic acid,
 78 formic acid, and methanol, albeit not in a catalytic fashion.²⁵
 79 More recently, Wehmschulte et al. reported the LA-catalyzed
 80 hydrosilylation of CO₂ by cationic aluminum species AlR₂⁺ (R
 81 = Et or OAr).²⁶ However, the detailed mechanism of such LA-
 82 catalyzed CO₂ reduction remains unclear, and thus further
 83 enhancing catalytic performance through modification of
 84 catalyst structure seems challenging. In this context, it is of
 85 great interest and importance to survey suitable main-group LA
 86 candidates for effective CO₂ reduction. Inspired by the dual
 87 activation of CO₂ and silane R₃SiH {SiH} by the above
 88 overviewed TM or TM/B(C₆F₅)₃ systems, we envisioned that a
 89 combination of the more oxophilic and higher Lewis acidic
 90 Al(C₆F₅)₃ {[Al]},²⁷ which could be sufficiently potent to render
 91 CO₂ fixation into silyl formate, with the less oxophilic B(C₆F₅)₃
 92 {[B]}, which favors FLP-type [SiH] activation for subsequent
 93 steps of reduction,²⁸ could serve as a main-group tandem FLP
 94 system that effectively converts CO₂ to CH₄. The tunability of
 95 [Al]/[B] catalysts should allow us to develop more efficient,
 96 economical, and recyclable tandem LA catalysts based on inter-
 97 or intramolecular and heterogeneous platforms. Accordingly,
 98 this contribution reports the first such main-group tandem LA
 99 catalytic system for highly effective and selective CO₂ reduction
 100 into CH₄ through hydrosilylation using a pair of [Al] and [B]
 101 LAs (Chart 1) which, when each used only, is ineffective (in

Chart 1. Proposed Fundamental Steps Involved in the Mixed Main-Group [Al]/[B] LA System for Tandem Catalytic Hydrosilylation of CO₂ into CH₄



102 case of [B]) or only marginally effective (in case of [Al]) for
 103 catalyzing this transformation. In this context, we present
 104 herein a full account of our combined experimental and
 105 theoretical/computation investigations into this novel main-
 106 group [Al]/[B] tandem catalyst system.

107 ■ RESULTS AND DISCUSSION

108 **Fixation of CO₂ with {Et₃SiH + [Al]} and Selective**
 109 **Reduction of CO₂ to CH₄ by {Et₃SiH + [Al]/[B]}.** As [B] was
 110 shown to be ineffective in catalyzing reduction of CO₂ via
 111 hydrosilylation,²⁹ we turned our attention to [Al], a stronger
 112 LA based on several lines of experimental and theoretical
 113 evidence.^{27,30} Most recently, we have revealed that the Al
 114 center of the even unsolvated Al(C₆F₅)₃ is not truly
 115 tricoordinated, but it adopts a dimeric structure with double
 116 Al...F(*ortho*) interactions in solid state.³¹ Such weak
 117 interactions are readily destroyed by addition of more
 118 electron-donating substrates than [Al] itself, such as toluene,
 119 ferrocene, or even fluorosilane and hydrosilane.^{30a,31,32} For
 120 instance, the unsolvated [Al] forms a stable and isolable adduct

with Et₃SiH in hexanes, while the interaction between [B] and
 Et₃SiH could only be detected by indirect spectroscopic
 evidence.^{28h} These observations suggest that the activation of
 the Si-H bond by [Al] is stronger than by [B]. However, the
 hydrosilylation of ketones by Et₃SiH proceeds more efficiently
 with [B] than with [Al], due to the high Lewis acidity and
 oxophilicity of [Al] that favor its complexation with the ketone
 substrates, greatly suppressing the Si-H bond activation. On
 the other hand, the feasible dissociation between the carbonyl
 substrates and [B] (even at a small ratio) enables the activation
 of the Si-H bond by the free [B] and the subsequent
 hydrosilylation.^{28j} Notably, Stephan et al. showed that [Al]
 reacts with CO₂ at 90 °C to form a dimeric Al compound
 [(C₆F₅)C(O)OAl(C₆F₅)₂]₂ by insertion of CO₂ into the Al-
 C₆F₅ bond,³³ while Müller reported that a [Si-H...Al] system
 with a coordinatively saturated, less Lewis acidic aluminum
 center is inactive for CO₂ fixation.³⁴

Excitingly, the stoichiometric reaction between [Et₃SiH·
 Al(C₆F₅)₃] and CO₂ at room temperature (RT) (entry 1, Table
 1) revealed the rapid disappearance of the silane Si-H signal at

Table 1. Selected Results of CO₂ Reduction via Hydrosilylation by [Al] and [Al]/[B]

entry	silane	cat.	conditions	[SiH] conv. (%) ^a	CH ₄ yield (%) ^b
1	Et ₃ SiH	–	12 h, 80 °C	0	0
2	Et ₃ SiH	5% [B]	12 h, 80 °C	2	0
3	Et ₃ SiH	100% [Al]	1 h, RT	98	0
4a	Et ₃ SiH	10% [Al]	10 h, 80 °C	39	14
4b	Et ₃ SiH	10% [Al]	24 h, 80 °C	54	16
5	Et ₃ SiH	5.0% [Al] + 5.0% [B]	1 h, RT	15	7
6	Et ₃ SiH	5.0% [Al] + 5.0% [B]	5 h, 80 °C	100	82

^aBased on silane consumption. ^bSee the SI for yield calculation details.

3.75 ppm and concomitant appearance of new signals at 8.17
 ppm in ¹H NMR, at 172.8 ppm in ¹³C NMR, and at 46.0 ppm
 (downfield shifted from 0.0 ppm from the silane) in ²⁹Si NMR
 (Figure 1). These spectroscopic features are consistent with the
 generation of a complexed silyl formate species, which was
 identified as the complex HCOOSiEt₃-[Al] (1-[Al]), the
 structure of which was confirmed by single-crystal X-ray
 diffraction (SC-XRD) analysis (Chart 2). No further reduction
 to lower oxidation state species was detected. With 10 mol % of
 [Al], the generation of 1-[Al] (10% based on Et₃SiH) was
 observed, but no further silane conversion was achieved. Other
 silanes such as ^tPr₃SiH and PhMe₂SiH also led to the formation
 of the corresponding silyl formate-[Al] complexes (see the
 Supporting Information). These observations suggest that the
 activation of CO₂ by [Al] likely occurs through the typical LA-
 carbonyl activation and the LA is not released from the
 resulting product under these conditions, thus requiring a
 stoichiometric amount of LA. To render this reaction catalytic
 and possibly promote further hydrosilylation of the formed
 intermediates, we heated the above mixture to 80 °C for 24 h,
 achieving a moderate conversion of 54% (calculated from the
 silane consumption) with a 16% CH₄ yield (entry 4b, Table 1).
 These results imply that the catalytic performance of [Al]
 decreases as the basicity of the subsequent reaction

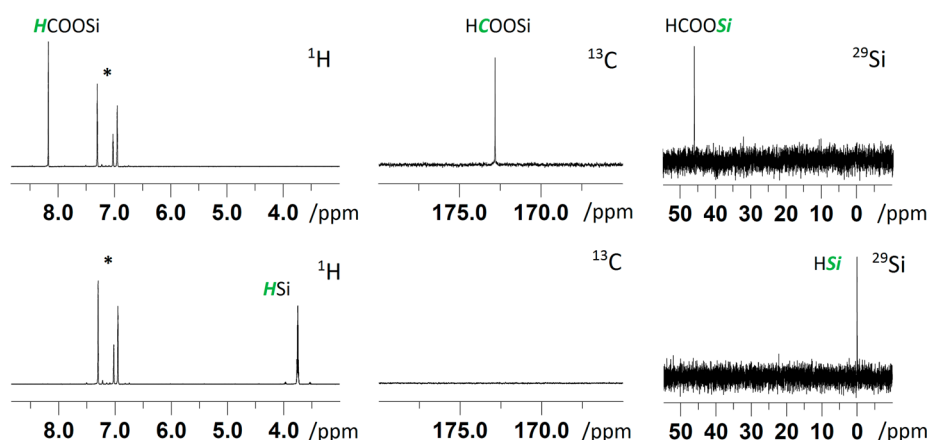
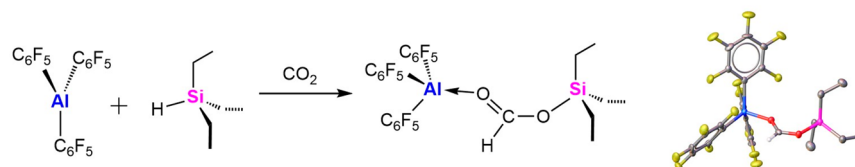
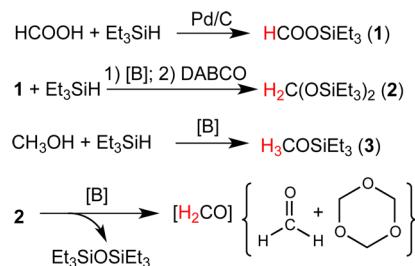


Figure 1. Comparisons of ^1H , ^{13}C , and ^{29}Si NMR spectra before (bottom) and after (top) CO_2 fixation by $[\text{Et}_3\text{SiH} + \text{Al}(\text{C}_6\text{F}_5)_3]$ in $\text{C}_6\text{D}_5\text{Br}$ at 25°C .

Chart 2. CO_2 Insertion into Si–H Bond with the $[\text{Et}_3\text{SiH} + \text{Al}(\text{C}_6\text{F}_5)_3]$ System To Form the $[\text{Al}]$ -Coordinated Silyl Formate and the Corresponding Solid-State Structure Determined by SC-XRD



Scheme 1. Preparation of the Reaction Intermediates Involved in the Overall CO_2 Reduction Cycle



sequestration of the $[\text{B}]$ catalyst to prevent further hydro-180
silylation is necessary.^{16a} Interestingly, in our attempts to 181
reduce HCOOSiEt_3 with 1 equiv of Et_3SiH , we observed 182
selective formation of $\text{H}_2\text{C}(\text{OSiEt}_3)_2$ in 5 min, after which the 183
product gradually underwent further rearrangement to form 184
1,3,5-trioxane (a formaldehyde equivalent) and hexaethyldisi-185
loxane $\text{Et}_3\text{SiOSiEt}_3$. This process is believed to proceed through 186
coordination of the catalytic amount of $[\text{B}]$ to the substrate, as 187
sequestration of $[\text{B}]$ with DABCO (1,4-diazabicyclo[2.2.2]-188
octane) prevented the aforementioned rearrangement reaction 189
and enabled the isolation of $\text{H}_2\text{C}(\text{OSiEt}_3)_2$. In a separate NMR 190
scale experiment, $\text{H}_2\text{C}(\text{OSiEt}_3)_2$ was left for 1 day in $\text{C}_6\text{D}_5\text{Br}$ 191
and remained intact, but addition of 5 mol % of $[\text{B}]$ converted 192
 $\text{H}_2\text{C}(\text{OSiEt}_3)_2$ into 1,3,5-trioxane and $\text{Et}_3\text{SiOSiEt}_3$ in 1 h 193
(Figures S21 and S22). Indeed, the formation of the 194
formaldehyde intermediate even without a catalyst is energeti-195
cally feasible for bis(phenylsilyl)acetal $\text{H}_2\text{C}(\text{OSiH}_2\text{Ph})_2$, via 196
intramolecular elimination of $\text{PhH}_2\text{SiOSiH}_2\text{Ph}$, as predicted by 197
calculations reported by Wang et al.³⁵ Our proposed 198
mechanism through coordination of $\text{H}_2\text{C}(\text{OSiEt}_3)_2$ to $[\text{B}]$ 199
will be discussed in the following sections. The final disiloxane 200

intermediates $[\text{HCOOSiEt}_3, \text{H}_2\text{C}(\text{OSiEt}_3)_2, \text{and } \text{H}_3\text{COSiEt}_3,$ 165
vide infra] increases. Intriguingly, when we employed a mixed 166
LA system containing 5 mol % $[\text{Al}] + 5$ mol % $[\text{B}]$, quantitative 167
conversion of the silane with 82% CH_4 yield was achieved at 80 168
 $^\circ\text{C}$ in 5 h (entry 6, Table 1; Figure 2). 169

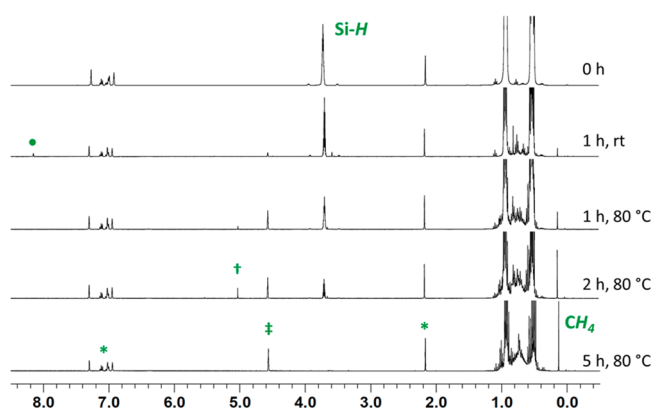


Figure 2. ^1H NMR (25°C , $\text{C}_6\text{D}_5\text{Br}$) spectra of hydrosilylation of CO_2 catalyzed by the mixed $[\text{Al}]/[\text{B}]$ system (entries 3 and 4, Table 1) at different time intervals (●: HCOOSiEt_3 - $[\text{Al}]$, ‡: $\text{H}_2\text{C}(\text{OSiEt}_3)_2$ - $[\text{Al}]$, †: free $\text{H}_2\text{C}(\text{OSiEt}_3)_2$ and *: toluene from $[\text{Al}]$ and NMR solvent residue).

Isolation of Reaction Intermediates. To elucidate the 170
possible mechanism for this unique $[\text{Al}]/[\text{B}]$ tandem catalyst 171
system, we synthesized each of the intermediates or byproducts 172
involved in the above reduction scheme, including HCOO -173
 SiEt_3 , $\text{H}_2\text{C}(\text{OSiEt}_3)_2$, $\text{H}_3\text{COSiEt}_3$, and $\text{Et}_3\text{SiOSiEt}_3$ (Scheme 1). 174
Compounds HCOOSiEt_3 and $\text{H}_3\text{COSiEt}_3$ were readily 175
prepared from the dehydrogenative coupling of the correspond-176
ing precursors by Pd/C or $[\text{B}]$.^{26b} On the other hand, 177
successful examples or selective formation and isolation of 178
 $\text{H}_2\text{C}(\text{OSiEt}_3)_2$ remain scarce.^{5a,15,16} Piers et al. noted that the 179

Scheme 2. Binding Interaction of Each Intermediate with [Al] and [B] Catalysts

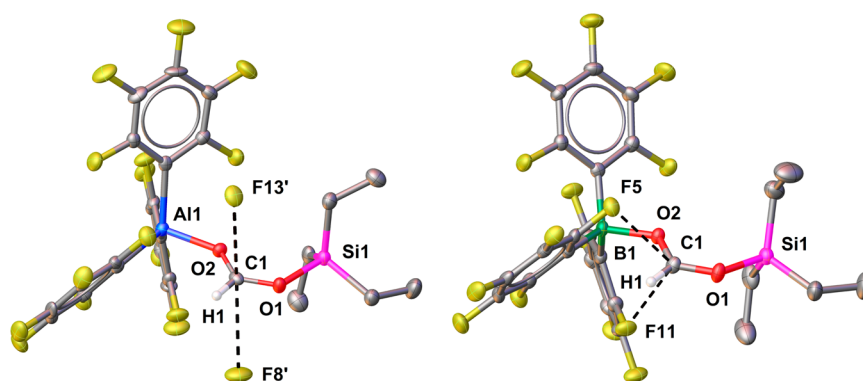
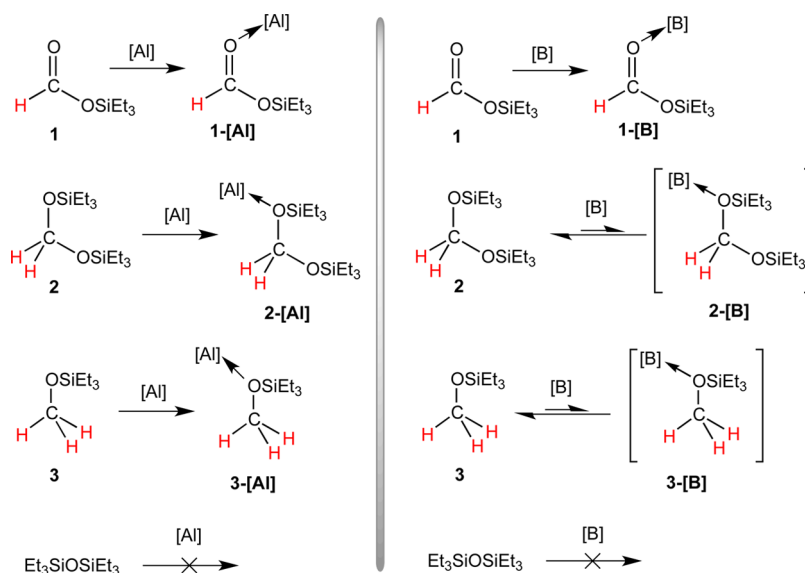


Figure 3. X-ray crystal structures of 1-[Al] and 1-[B] with thermal ellipsoids drawn at the 50% probability. Hydrogen atoms except H1 were omitted for clarity. Selected bond lengths (Å) and angles (deg) for 1-[Al]: C1–O1 1.277(2), C1–O2 1.242(2), Al1–O2 1.8532(16), Si1–O1 1.7717(15), C1···F8' 2.935(3), and C1···F13' 2.908(3); for 1-[B]: C1–O1 1.276(2), C1–O2 1.245(2), B1–O2 1.621(2), Si1–O1 1.7499(14), C1···F5 2.838(3), and C1···F11 2.748(2).

203 Binding Interaction between the Intermediates and

204 [Al] or [B]. With all three intermediates in hand, we studied
 205 their interaction with [Al] and [B] (Scheme 2). As expected,
 206 the less sterically hindered HCOOSiEt₃ forms a stable adduct
 207 with both [Al] and [B]. Crystalline 1-[Al] and 1-[B] adducts
 208 can be isolated in pure form by crystallization of equimolar 1
 209 and [Al] or [B] in hexanes at –35 °C. Further supporting
 210 evidence came from multinuclear spectroscopic data (Figures
 211 S1–9) chiefly: (1) the aldehyde proton appears at 8.17 and
 212 7.95 ppm in ¹H NMR for 1-[Al] and 1-[B], respectively; (2)
 213 the ¹⁹F NMR spectra also exhibit typical patterns for
 214 tetracoordinate aluminum and boron species; (3) both the
 215 formate and the LA signals are present in the ¹³C NMR and
 216 assigned; and (4) the ²⁹Si NMR signals are significantly
 217 downfield shifted for 1-[Al] (δ 46.0 ppm) and 1-[B] (δ 46.4
 218 ppm) when compared to the free 1 (δ 26.6 ppm). Worth
 219 noting here is that the spectroscopic data of 1-[Al] is consistent
 220 with those generated by the stoichiometric reaction between
 221 CO₂ and [Et₃SiH·Al(C₆F₅)₃].

222 The direct structural evidence for the 1:1 complexation in 1-
 223 [Al] and 1-[B] was derived from the SC-XRD analysis (Figure
 224 3). In the structure of 1-[Al], the Al–O2 bond is rather strong,
 225 as indicated from the short bond length of 1.8532(16) Å.

Notably, the C1–O2 and C1–O1 distances are 1.242(2) and 226
 1.277(2) Å. This specific alternation suggests that C1–O2 227
 features a more double-bond character, while C1–O1 features a 228
 more single-bond character. In another word, if 1-[Al] is 229
 viewed as a model in which [Al] and [Si]⁺ are competing for 230
 the middle formate anion, then [Si]⁺ exhibits stronger 231
 interaction with the anion. Nonetheless, both C1–O2 and 232
 C1–O1 distances are shorter than the typical C–O single bond 233
 (cf. 1.43 Å) and longer than the C=O double bond (cf. 1.23 234
 Å), indicative of a certain degree of conjugated resonance 235
 structure along the –O1–C1–O2– moiety. The middle C1 236
 carries a partial positive charge, accounting for the further 237
 secondary interactions with two *para*-F atoms [C1···F contact: 238
 2.908(3) and 2.935(3) Å] from two neighboring molecules. 239
 The structural parameters for 1-[B] are overall similar to those 240
 of 1-[Al]: C1–O1 1.276(2), C1–O2 1.245(2), B1–O2 241
 1.621(2), except that secondary C···F contacts [2.748(2) and 242
 2.838(3) Å] were derived from an intramolecular fashion with 243
 the adjacent –C₆F₅ ring instead, presumably due to the smaller 244
 radius of boron and shorter bond lengths around it. Further 245
 evidence for activation of the carbonyl moieties by LAs was 246
 deduced from FT-IR analysis of the solid samples of 1-[Al] and 247
 1-[B] (Figure S32). When compared with the uncoordinated 1 248

Scheme 3. Catalytic Hydrosilylation Reaction of Each Fundamental Step

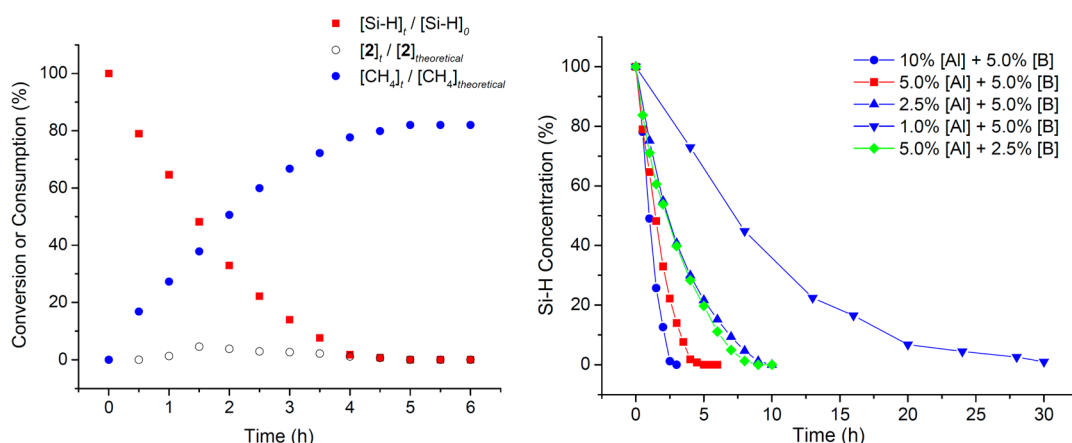
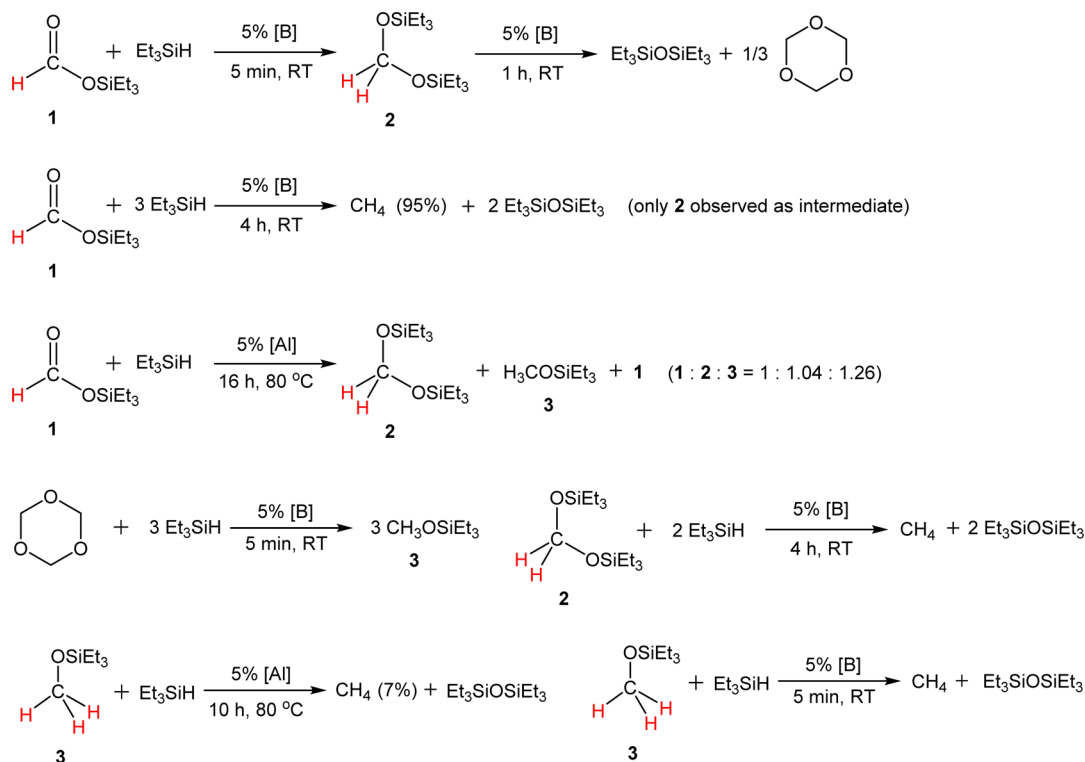


Figure 4. Kinetic plots under current standard conditions (left, 80 °C, 5 mol % [Al], and 5 mol % [B]) and varied loading of [Al] and [B] (right).

249 (cf. 1798 cm^{-1}), both $\mathbf{1}$ -[Al] (1604 cm^{-1}) and $\mathbf{1}$ -[B] (1597
250 cm^{-1}) exhibit significant shifts of the C=O stretching mode to
251 lower frequencies by 204 and 211 cm^{-1} , respectively.

252 In contrast, the interaction of [Al] and [B] with the bulkier
253 and less basic $\text{H}_2\text{C}(\text{OSiEt}_3)_2$ and $\text{H}_3\text{COSiEt}_3$ is different (see
254 Scheme 2 and SI). In the case of the more sterically hindered
255 and less acidic [B] (relative to [Al]), there was no spectral
256 change from the ^1H NMR signals for its 1:1 mixture with
257 $\text{H}_2\text{C}(\text{OSiEt}_3)_2$ or $\text{H}_3\text{COSiEt}_3$. However, based on the fact that
258 $\text{H}_2\text{C}(\text{OSiEt}_3)_2$ readily undergoes the rearrangement reaction in
259 the presence of [B] in a prolonged period, it is likely that [B]
260 can bind to $\text{H}_2\text{C}(\text{OSiEt}_3)_2$, albeit in a very weak fashion that
261 favors the dissociated form. Given that the bulkiness of
262 $\text{H}_3\text{COSiEt}_3$ is less than that of $\text{H}_2\text{C}(\text{OSiEt}_3)_2$, it is plausible that
263 [B] can also bind to $\text{H}_3\text{COSiEt}_3$ reversibly, even though the ^1H
264 data again indicated that this equilibrium strongly favors the
265 dissociated form. To the contrary, the NMR scale reaction

between [Al] and $\text{H}_2\text{C}(\text{OSiEt}_3)_2$ or $\text{H}_3\text{COSiEt}_3$ results in
266 spectral shifts in the ^1H signals, corresponding to complexation
267 between [Al] and $\text{H}_2\text{C}(\text{OSiEt}_3)_2$ or $\text{H}_3\text{COSiEt}_3$. In particular,
268 [Al] forms isolable crystalline complex with $\text{H}_3\text{COSiEt}_3$. We
269 tried to perform SC-XRD analysis of the complex but failed to
270 obtain satisfactory results after several attempts due to poor
271 crystal quality. Nonetheless, the overall molecular skeleton and
272 atom connectivity of this adduct could be recognized from the
273 crude data (Figure S34). Collectively, these observations
274 further support that in the subsequent reduction of lower-
275 oxidation-state species HCOOSiEt_3 , $\text{H}_2\text{C}(\text{OSiEt}_3)_2$, and
276 $\text{H}_3\text{COSiEt}_3$, [B] should serve as a better catalyst than [Al]
277 due to the weaker substrate–catalyst interaction, which
278 facilitates the FLP-type Si–H activation. In addition, the
279 byproduct $\text{Et}_3\text{SiOSiEt}_3$ does not form a detectable adduct with
280 either [B] or [Al], which enables [Al] and/or [B] to re-enter
281 the catalytic cycle after the last step (CH_4 generation). 282

283 **Kinetic and Mechanistic Studies of Hydrosilylation of**
 284 **CO₂.** To further address our hypothesis on the catalytic roles of
 285 each LA in the current mixed tandem [Al]/[B] system, we
 286 carried out a kinetic study on each step of the hydrosilylation
 287 (Scheme 3), coupled with a computational investigation (vide
 288 infra). As described previously, in step 1, the fixation of CO₂ is
 289 mediated by [Al] to form 1-[Al]. The following hydrosilylation
 290 steps 2–4 proceed more efficiently with [B] than with [Al].
 291 Among them, the reactions of HCOOSiEt₃ or H₃COSiEt₃ with
 292 1.0 equiv of Et₃SiH in the presence of 5 mol % [B] were
 293 completed within 5 min at RT, while the slowest step, the
 294 hydrosilylation of H₂C(OSiEt₃)₂ under similar conditions
 295 generated a mixture of unreacted H₂C(OSiEt₃)₂, CH₄, and a
 296 trace amount of H₃COSiEt₃. Nonetheless, treatment of
 297 HCOOSiEt₃ with 3.0 equiv of Et₃SiH and 5 mol % [B]
 298 resulted in full conversion to CH₄ in 4 h, during which
 299 H₂C(OSiEt₃)₂ accumulates as the detectable intermediate. In
 300 addition, the reduction of 1,3,5-trioxane with 1.0 equiv of
 301 Et₃SiH and 5 mol % [B] led to exclusive formation of
 302 H₃COSiEt₃, indicating that the hydrosilylation of trioxane is
 303 even faster than that of H₃COSiEt₃. In comparison, the
 304 hydrosilylation of the related substrates with [Al] at RT is not
 305 effective at all and only provided a trace amount of the
 306 reduction products, but at 80 °C after longer times some
 307 hydrosilylation products were observed (Scheme 3)

308 To gain further insights of such tandem hydrosilylation of
 309 CO₂, we carried out a kinetic study of the overall reduction
 310 process. Under our standard conditions (entry 6, Table 1), the
 311 reaction was complete in 5 h. Et₃SiH consumption and CH₄
 312 yield at the early stage of the reaction showed a linear
 313 relationship with time (Figure 4). The concentration of
 314 detectable intermediate H₂C(OSiEt₃)₂ (2) reached a plateau
 315 at 1.5 h and then decreased gradually. The maximum turnover
 316 frequency (TOF) of the consumption of [SiH] using the first 5
 317 data points from the initial 2 h was calculated to be 6.6 h⁻¹, and
 318 the rate for the [SiH] conversion was $r_{\text{SiH}} = 0.13 \text{ M h}^{-1}$.
 319 Variation of the [Al] catalyst concentration (from 1.0 mol % to
 320 10 mol %, Table 2) greatly impacted the [SiH] consumption
 321 rate. Overall, the reduction rate of CO₂, as monitored by the
 322 consumption of [SiH] signal, was proportional to the [Al]
 323 loading. The only observed species at δ 4.75 ppm after
 324 complete [SiH] conversion was the 2-[Al] adduct, which is
 325 consistent with the stoichiometric reaction between 2 and [Al].

Table 2. Selected Results of CO₂ Hydrosilylation at 80 °C under Different Tandem Catalyst Loadings

catalyst composition	reaction time (h) ^a	max TOF (h ⁻¹) ^b	r_{SiH} (M h ⁻¹) ^c	conv. (%) ^d	CH ₄ yield (%) ^e
10% [Al] + 5.0% [B]	3	5.0	0.20	100	77
5.0% [Al] + 5.0% [B]	5	6.6	0.13	100	82
2.5% [Al] + 5.0% [B]	10	7.9	0.079	100	91
1.0% [Al] + 5.0% [B]	30	6.03	0.024	99	94
5.0% [Al] + 2.5% [B]	9	7.85	0.0785	100	80

^aBased on [SiH] consumption from ¹H NMR measurement. ^bBased on the steepest slope from the linear fit of conversion against time at the early stage of hydrosilylation, see Figures S27–S31. ^cRate of [SiH] consumption, calculated based on max TOF. ^dBased on [SiH] consumption. ^eSee the SI for yield calculation details.

As expected, lowering the [Al] loading reduced the amount of the final 2-[Al] residue and hence improved the yield of CH₄. In addition, decreasing the [B] concentration also resulted in a decrease of CO₂ reduction rate. Remarkably, when only 1.0 mol % of [Al] was employed, the highest CH₄ yield of 94% was achieved (Table 2).

Collectively, the above results showed that CO₂ fixation is promoted by [Al], while the subsequent hydrosilylation reactions are catalyzed by [B]. To further clarify the preferred pathway of each step, namely conventional carbonyl activation versus FLP-type silane activation, and to explain the observed activity for the CO₂ reduction into CH₄ by [Al] alone but requiring 80 °C for 24 h (entries 2a-b, Table 1), albeit being much less effective than the mixed [Al]/[B] tandem catalyst system, we performed the following additional experiments. We first mixed equimolar 1-[B] and Et₃SiH-[Al], which resulted in the instantaneous replacement of Et₃SiH by HCOOSiEt₃ to form 1-[Al]. However, the subsequent hydrosilylation was hindered, as only a trace amount of 2-[Al] was detected up to 1 h, in contrast to the rapid reduction of 1-[B] by Et₃SiH in the absence of [Al]. This observation is in line with the Si–H activation mechanism, in which the free carbonyl has to be formed to initiate the attack at the Si center of a transient H···[B] intermediate. If the carbonyl is coordinated to an additional LA, [Al], such nucleophilic attack becomes less plausible. With this premise, we gratifyingly found that heating the mixture to 80 °C led to the formation of 2-[Al], due to thermally induced dissociation of HCOOSiEt₃ from [Al], enabling its reduction to H₂C(OSiEt₃)₂ that recombines with [Al] to form 2-[Al]. Addition of an excess amount of Et₃SiH into such a mixture further converted H₂C(OSiEt₃)₂ to CH₄ at 80 °C. In a similar fashion, addition of [Al] to a mixture of H₃COSiEt₃, [B] and Et₃SiH reduced the hydrosilylation rate of H₃COSiEt₃ to CH₄. These experiments further confirm that the reduction steps 2–4 occur through the FLP Si–H activation mechanism, and a higher temperature is necessary to facilitate the release of substrates (1, 2, and 3) from [Al], which also renders [Al] catalytic by reentering the catalytic cycle for the step 1 reduction.

In order to investigate the catalyst recyclability, the catalytic system consisting of 10 mol % [Al] and 5.0 mol % [B] was tested for 3 cycles. In the first cycle, the hydrosilylation was complete in 3 h (Figure 5). After careful removal of excess CO₂ and CH₄ under vacuum, the system was recharged with the same amount of Et₃SiH and CO₂ as in the first cycle. The hydrosilylation of the second and third cycles was complete in 6 and 14 h, respectively. This recycling experiments indicated that the [Al]/[B] catalysts survived during catalytic cycle and are recyclable. Although we detected the decrease in catalyst efficiency from cycle to cycle (presumably due to partial hydrolysis of the catalyst during the reloading of CO₂), quantitative conversion can still be achieved on the third load of Et₃SiH and CO₂.

Computational Studies of Fundamental Steps 1–4.³⁶

In this section we discuss each reduction step separately starting from the hydrosilylation of CO₂ to formate and ending with the hydrosilylation of methyl silyl ether to methane. In Schemes 4, 5, and 6 numbers in green refer to [Al], while numbers in blue refer to [B]. Further, to strengthen connections with experiments, we labeled DFT structures using letters, such as A, B, C, etc., while for structures involving intermediates 1–3 we kept the same labeling scheme as that used in the description of the experimental results.

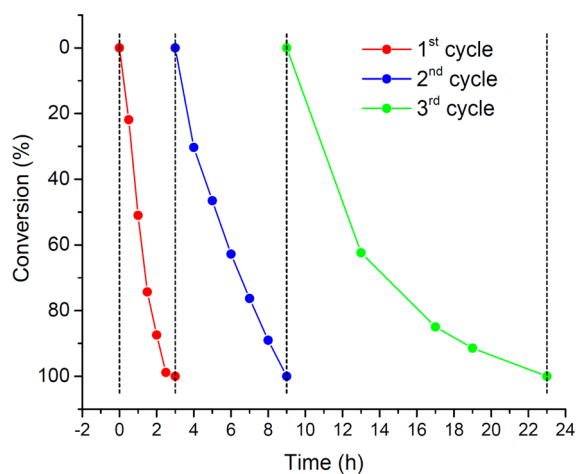


Figure 5. Recyclability of CO₂ reduction with 10 mol % [Al] and 5.0 mol % [B]. Reaction time for complete SiH consumption in each cycle: 3, 6, and 14 h.

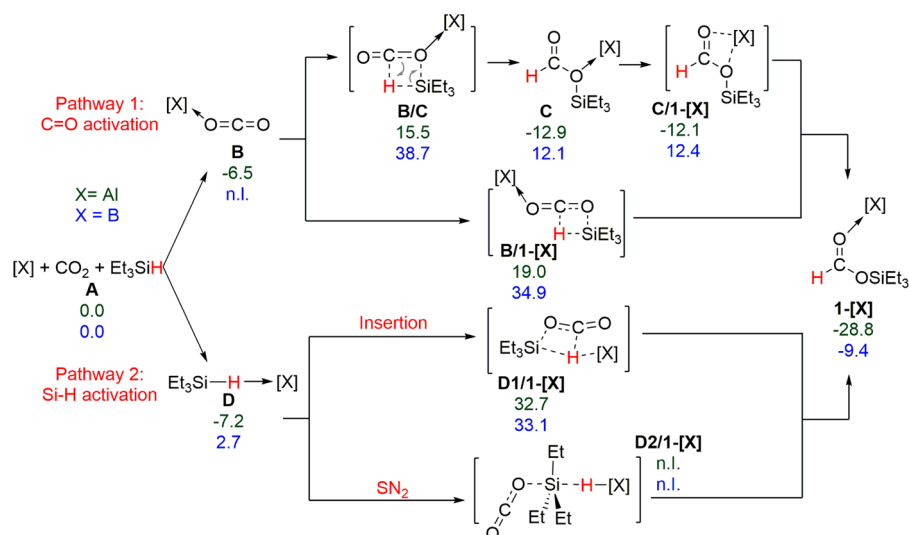
389 *Step 1: Hydrosilylation of CO₂ to Silylformate 1-[X]* (X =
390 Al, B). The two possible reaction pathways we investigated to
391 generate **1** from CO₂ are reported in [Scheme 4](#).

392 Along pathway 1 the individual LA directly activates the CO₂
393 molecule toward the H-transfer from Et₃Si-H. Pathway 2,
394 instead, starts with a FLP-type Si-H activation with
395 coordination of Et₃SiH to the LA, followed by the H-transfer
396 to the CO₂ molecule through an insertion mechanism or a SN₂
397 transition state and by rearrangement of the initially formed
398 [OCOSiEt₃]⁺/[H-LA]⁻ ion pair. Focusing on pathway 1, in the
399 case of [B] we were not able to locate a CO₂-B(C₆F₅)₃ adduct,
400 **B**. Nevertheless, we found two possible four-membered
401 transition states, **B/C** and **B/1-[X]** in [Scheme 4](#), where the
402 silicon attacks one oxygen of CO₂ favoring the simultaneous H-
403 transfer from Et₃Si-H to the CO₂ carbon atom. Transition
404 state **B/C** collapses into intermediate **C** before reaching **1-[X]**,
405 favored by 9.4 kcal/mol, while transition state **B/1-[X]**
406 collapses directly into product **1-[X]**. The energy cost to
407 reach transition states **B/1-[X]** and **B/C**, around 35–39 kcal/

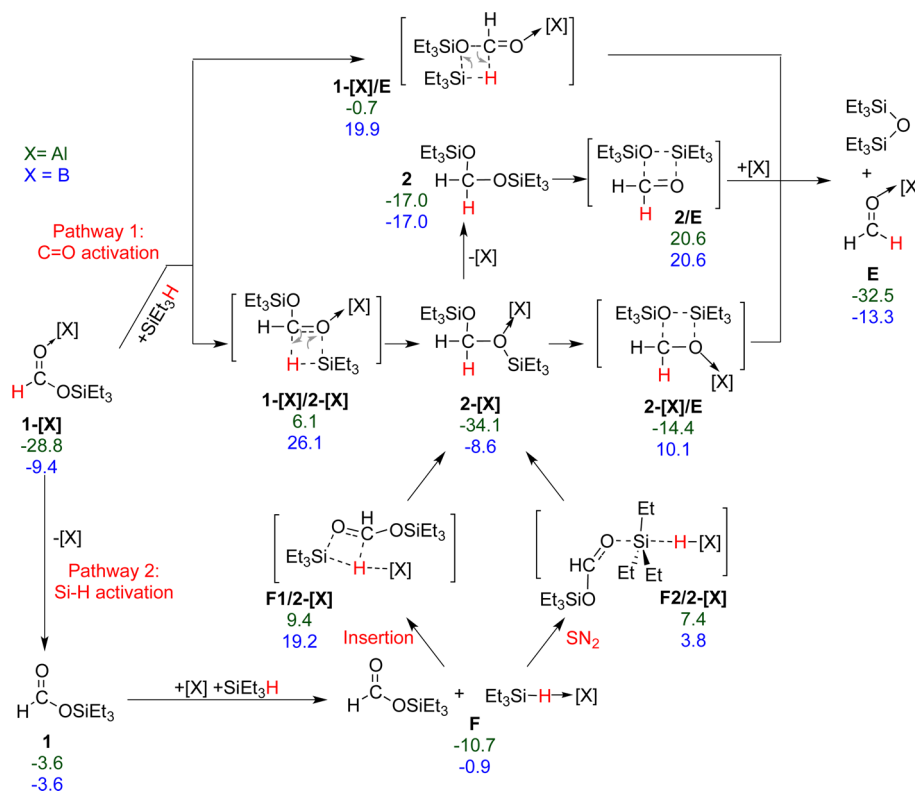
mol, **and** the fact that these transition states should be formed
by the encounter of three molecules due to the instability of the
preformed **B** intermediate explain the experimentally observed
inability of [B] to activate CO₂. Conversely, the CO₂-alane
adduct **B** was located 6.5 kcal/mol below separated Al(C₆F₅)₃
and CO₂. This interaction weakens the C=O bond of the CO₂
moiety, as shown by the slightly elongated C=O bond distance
(1.19 Å in **B** vs 1.17 Å in the free CO₂). [Al] coordination
results in an increased positive charge on the C atom of the
CO₂ moiety (1.07e in **B** vs 0.99e in the free CO₂), promoting
the H-transfer from Et₃SiH to the electrophilic C center. This
H-transfer occurs via the four-membered transition state **B/C**,
with the [Al] coordinated O atom attacking the Si atom and an
energy barrier of 22.0 kcal/mol. Transition state **B/C** collapses
into intermediate **C**, which can further precipitate in the final
product **1-[X]** (ΔG = -28.8 kcal/mol) through the almost
barrier-less transfer of the [Al] to the carbonyl oxygen, via
transition state **C/1-[X]**. The alternative transition state with
the uncoordinated O atom of **B** attacking the Si atom, **B/1-[X]**,
and leading to **1-[X]** directly, was located 3.5 kcal/mol above
B/C. The stability of the CO₂-[Al] adduct **B** and the low-
energy barrier of 22.0 kcal/mol explain the experimentally
observed capability of [Al] to activate CO₂.

As for the competitive mechanism via Si-H activation,
pathway 2 in [Scheme 4](#), it involved the formation of a silane-LA
adduct. Formation of such adduct was found to be favored by
7.2 kcal/mol with [Al], whereas in the case of [B] it is
disfavored by 2.7 kcal/mol. The transition state for the
following insertion of CO₂ into the Si-H bond, **D1/1-[X]** in
[Scheme 4](#), lies at 32.7 kcal/mol for [Al] and 33.1 kcal/mol for
[B]. Finally, we also tried to promote Si-H activation via the
SN₂-type transition state **D2/1-[X]**, corresponding to the
concerted attack of the CO₂ oxygen to the silicon atom and
transfer of the H atom to the [X] moiety. However, we were
not able to locate this kind of transition state for both [Al] and
[B]. Overall, calculations confirmed the experimental inefficiency
of [B] in the first step of CO₂ hydrosilylation, since [B] is
not able to effectively activate CO₂ through either direct
coordination to CO₂ or FLP-type silane activation. As far as
[Al] is concerned, calculations suggest that the reduction of

Scheme 4. Hydrosilylation of CO₂ to the Silylformate Complex **1-[X]**^a



^aFree energies (kcal/mol) in *n*-Hexane are reported for X = Al (numbers in green) and B (numbers in blue) (n.l. = not located).

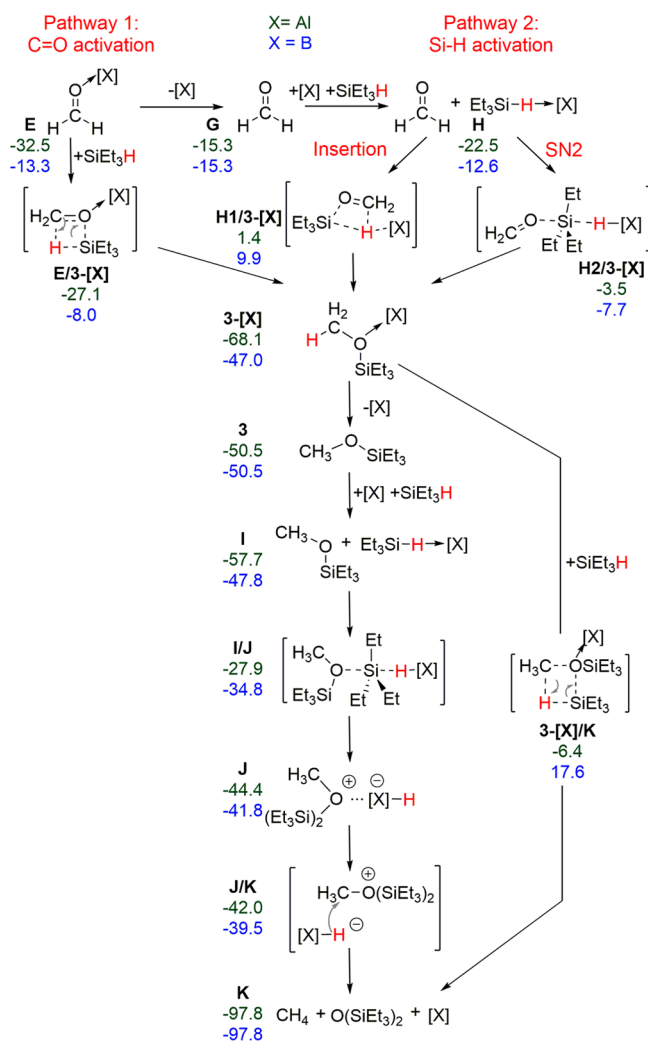
Scheme 5. Hydrosilylation of Silylformate 1-[X] to H₂C(OSiEt₃)₂/Formaldehyde^a

^aFree energies (kcal/mol) in *n*-hexane are reported for X = Al (numbers in green) and B (numbers in blue).

448 CO₂ to silylformate occurs via CO₂ activation, whereas the
 449 pathway involving the FLP-type Si–H activation was ruled out.
 450 **Steps 2 and 3a: Hydrosilylation of Silylformate 1-[X] to**
 451 **H₂C(OSiEt₃)₂ (Step 2) and Formaldehyde (Step 3a).** Starting
 452 from the LA-silylformate adduct 1-[X], we studied the
 453 mechanisms most likely operative in the second hydrosilylation
 454 step, namely from the silylformate adduct 1-[X] to
 455 formaldehyde. The pathways considered with the corresponding
 456 energetics are reported in Scheme 5. We considered the H-
 457 transfer step from a second Et₃SiH molecule to the starting 1-
 458 [X] via the same pathways considered above for hydrosilylation
 459 of CO₂. Specifically, we considered two transition states along
 460 the C=O activation pathway, i.e., 1-[X]/E and 1-[X]/2-[X],
 461 where the Et₃SiH molecule attacks the oxygen of the LA–O
 462 bond or the oxygen of the Si–O bond of 1-[X]. Transition
 463 state 1-[X]/E, leading directly to Et₃SiOSiEt₃ and the LA-
 464 aldehyde adduct, E in Scheme 5, is favored by roughly 6–7
 465 kcal/mol relative to transition state 1-[X]/2-[X], leading to
 466 adduct 2-[X], with the experimentally characterized
 467 CH₂(OSiEt₃)₂ intermediate 2 bound to the LA. In this
 468 conversion, the two LAs behave similarly, with an overall
 469 energy barrier through the favored transition state 1-[X]/E of
 470 roughly 29 kcal/mol. This relatively high-energy barrier can be
 471 ascribed both to the high steric pressure in this second
 472 hydrosilylation transition state (two molecules of silane plus
 473 one LA) and to the reduced electrophilicity of the formate
 474 carbon center with respect to that of CO₂, as revealed by the
 475 charges of these two C centers, i.e., 1.07e in CO₂ vs 0.74e in 1-
 476 [X]. Finally, formation of E from 1-[X] + Et₃SiH is exergonic
 477 by almost 4.0 kcal/mol for both LAs, which drives aldehyde
 478 formation. As for conversion of the experimentally character-
 479 ized intermediate 2-[X] to the formaldehyde adduct E, it can

proceed either in a single step through transition state 2-[X]/E 480
 or through a two-step pathway via dissociation of [X] from 2- 481
 [X], followed by the direct reductive elimination of Et₃SiOSiEt₃ 482
 from 2 to release the aldehyde via transition state 2/E, 483
 following a similar mechanism reported in literature.³⁵ 484
 According to our calculations, the one-step mechanism via 485
 transition state 2-[X]/E, with an overall energy barrier around 486
 20 kcal/mol, is clearly favored over the direct reductive 487
 elimination from 2. Nevertheless, dissociation of the LA from 488
 2-[X] releasing intermediate 2 is energetically favored with [B], 489
 actually representing the thermodynamic product of the 490
 reaction. 491

As for the Si–H activation pathway, it starts with the 492
 conversion of 1-[X] into 2-[X], with the steps from 2-[X] to E 493
 already being discussed above. Thus, we focus here on the 494
 pathway from 1-[X] to 2-[X]. We calculated first the energetics 495
 involved in the release of the LA from the silylformate adduct 496
 1-[X]. As expected, dissociation of [Al], with a ΔG of 25.2 497
 kcal/mol, is more expensive than dissociation of [B], with a ΔG 498
 of only 5.8 kcal/mol. Starting from the LA free species 1 and a 499
 preformed Et₃SiH-[X] adduct, we located both the transition 500
 states for the direct formate insertion into the Si–H bond, F1/ 501
 2-[X], and the direct H-transfer between Et₃SiH and the LA via 502
 SN₂-type reactivity, F2/2-[X]. Based on the energy of the H- 503
 transfer transition states, both the Si–H activation pathways we 504
 examined can be ruled out in the case of [Al], since transition 505
 states F1/2-[X] and F2/2-[X] are more than 35 kcal/mol 506
 above intermediate 1-[X], respectively. Conversely, the 507
 insertion Si–H activation pathway is isoenergetic with the 508
 C=O activation pathway in the case of [B] and, more 509
 relevantly, the SN₂ type H-transfer mechanism via transition 510
 state F2/2-[X] shows a barrier of only 13.2 kcal/mol. 511

Scheme 6. Hydrosilylation of Formaldehyde to Silyl Methanol and Then to Methane^a

^aFree energy (kcal/mol) in *n*-hexane are reported for X = Al (numbers in green) and B (numbers in blue).

can react with the third equivalent of Et₃SiH along the C=O 534
activation pathway via the low-energy H-transfer transition state 535
E/3-[X] with both the LAs considered, with an energy barrier 536
around 5 kcal/mol. Alternatively, the key intermediate 3-[X] 537
can also be reached from E along the Si-H activation pathway 538
after dissociation of the LA to reach intermediate G. As 539
calculated in the previous reaction sequences, dissociation of 540
[Al] from E is clearly endergonic, whereas it is favored with 541
[B]. The liberated formaldehyde can react with a Et₃SiH-LA 542
adduct, intermediate H, via the already considered insertion or 543
SN₂-type pathways, through transition states H1/3-[X] and 544
H2/3-[X], respectively. The insertion mechanism can be 545
excluded since the H1/3-[X] transition state is more than 20 546
kcal/mol higher in energy than transition state E/3-[X] for 547
both [Al] and [B]. As for the SN₂-type pathway, it is 548
competitive for [B], since transition state H2/3-[X] is almost 549
isoenergetic with transition state E/3-[X] along the C=O 550
activation pathway. Differently, it can be excluded for [Al] since 551
the transition state H2/3-[Al] is almost 25 kcal/mol higher in 552
energy than transition state E/3-[Al]. 553

Two different pathways were considered to generate 554
methane from 3-[X]. The first pathway is the one-step H- 555
transfer from the fourth equivalent of Et₃SiH molecule to the 556
carbon of the activated adduct 3-[X] (C-O activation 557
pathway) via transition state 3-[X]/K. This pathway can be 558
excluded, since it requires the overcome of an energy barrier 559
>60 kcal/mol (Scheme 6). The second pathway is a multistep 560
process and starts with release of the LA from 3-[X], which is 561
again strongly endergonic for [Al], whereas it is slightly 562
exergonic for [B] (3-[X] vs 3 for [Al] and [B] in Scheme 6). 563
After releasing LA from 3-[X], silyl methanol 3 proceeds to the 564
last hydrosilylation step, via SN₂-type transition state I/J 565
involving 3 and a Et₃SiH-LA adduct. This H-transfer step is rate 566
determining, with a barrier of 16.0 kcal/mol for [B] (calculated 567
from the most stable 3 + Et₃SiH + LA species) and of almost 568
40 kcal/mol for [Al] (calculated from the most stable 3-[X] + 569
Et₃SiH species). As a consequence and in agreement with the 570
experimental results, the [Al] catalyst is inactive also in this last 571
hydrosilylation step, which proceeds smoothly with the [B] 572
catalyst. The last H-transfer within the formal [CH₃O- 573
(Et₃Si)₂]⁺/[H-LA]⁻ adduct J to release methane via transition 574
state J/K is almost barrier-less. As expected, formation of 575
methane is thermodynamically favored by roughly 50 kcal/mol 576
with respect to the silyl methanol intermediate 3. For the sake 577
of simplicity, the insertion pathway is not reported for the 578
conversion of 3 to methane, since it involves clearly unfeasible 579
barriers, as discussed in the previous sections. 580

Alane vs Borane: Electronic and Steric Analysis. The 581
results reported in the previous sections showed that the 582
experimentally observed catalytic difference between [Al] and 583
[B] seems to be due to the much higher stability of the LA- 584
adducts with [Al] relative to [B], in intermediates 1-[X], 2-[X], 585
E, and 3-[X] (see Schemes 5 and 6), which reflects the difficult 586
release of the LA from the substrates and the high barrier for 587
the Si-H bond activation. Focusing on the named 588
intermediates, the relative stability of 1-[X], E and 3-[X] is 589
more than 10 kcal/mol higher for [Al] than [B], respectively. 590
This result reflects in the key transition states for Si-H 591
activation (i.e., F2/2-[X] and H2/3-[X]) lying much higher in 592
energy for [Al]. Moreover, 2-[X] is favored by -17.1 kcal/mol 593
with [Al] and disfavored by 8.4 kcal/mol with [B] relative to 2, 594
and 3-[X] is favored by -17.6 kcal/mol with [Al] and 595
disfavored by 3.5 kcal/mol with [B] with respect to 3 (the total 596

512 Focusing on the thermodynamic scenario, the stability of the 513
intermediates shown in Scheme 5 seems to correlate with the 514
different catalytic behavior in the presence of [Al] or [B]. In 515
fact, for [Al] the thermodynamic product is the H₂C(OSiEt₃)₂- 516
[Al] adduct 2-[X], which is favored by 1.6, 5.3, and 17.1 kcal/ 517
mol relative to E, 1-[X], and 2, respectively. As consequence, 518
liberation of [Al] to promote further reactivity is compromised. 519
On the contrary, intermediate 2 is the most stable species in the 520
presence of [B], followed by E, with 1-[X] and 2-[X] being 521
clearly much less stable. The different thermodynamic stability 522
of 2 and 2-[X] with [Al] and [B], together with the much lower 523
energy barrier via the Si-H activation pathway, renders the [B] 524
catalyst active in the reduction of silylformate to formaldehyde, 525
in agreement with the experimental results.

526 **Steps 3b and 4: Hydrosilylation of Formaldehyde to Silyl** 527
Methanol (Step 3b) and Then to Methane (Step 4). The 528
reaction pathways we considered for the last two steps to form 529
methane from the aldehyde-LA adduct E are reported in 530
Scheme 6 with the related energies. Since no favored 531
hydrosilylation pathway was located starting from 2 of Scheme 532
5, we focused on the aldehyde-LA adduct E that turns out to be 533
the crucial species for the course of the reaction. Intermediate E

Scheme 7. Four Fundamental Steps and Calculated Energy Barriers in the Proposed Complete Catalytic Cycle for the Hydrosilylation of CO₂ into CH₄ in the Presence of Mixed [Al] and [B] LAs

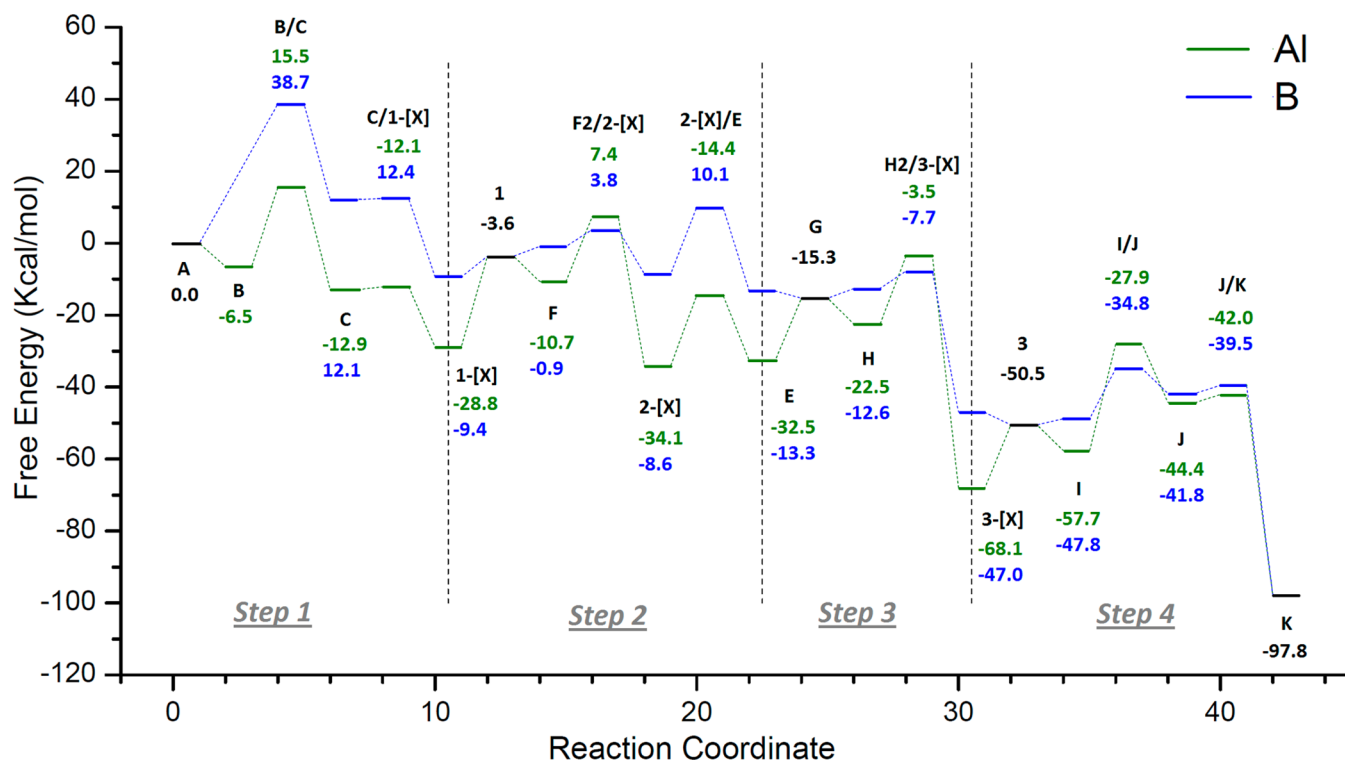
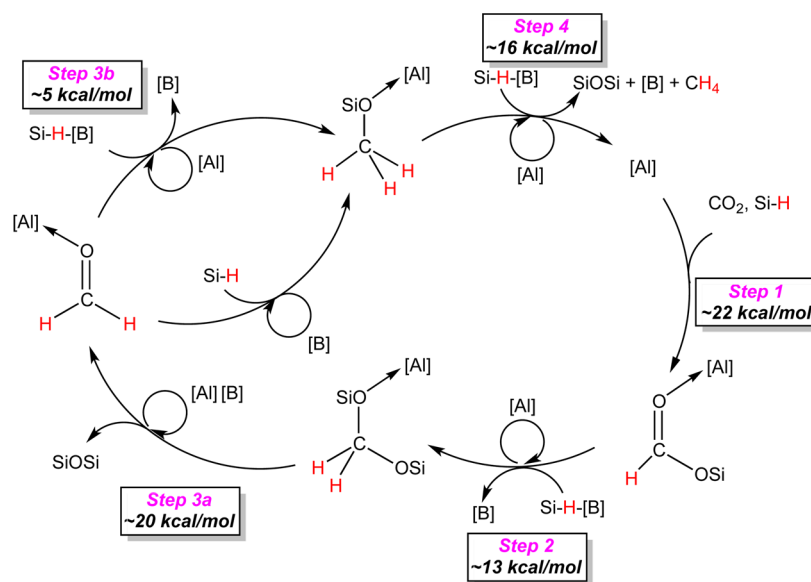


Figure 6. Calculated energy profiles of intermediates and transition states for [B] and [Al] pathways along the reaction coordinate.

597 difference between [Al] and [B] is of 25.5 and 21.1 kcal/mol,
598 respectively).

599 To better understand the large difference in the relative
600 stability of these intermediates, we analyzed both electronic and
601 steric effects. From an electronic point of view, the calculated
602 electrophilicity of the two LAs (0.24 for [Al] and 0.38 for [B])
603 appears to indicate that the formation of [B]-adducts should be
604 favored relative to the formation of [Al]-adducts. Indeed, the
605 relative energies of the SN₂ H-transfer transition states relative
606 to the preceding intermediates are in line with the electro-
607 philicity results. Moving to sterics, we tested the relative

608 stability of 2 and 3 with respect to 2-[X] and 3-[X] with XH₃
609 (X = Al and B) as LA. The difference in the binding energy of 2
610 and 3 to AlH₃ and BH₃ is only 2.7 and 4.5 kcal/mol, relative to
611 a difference >20 kcal/mol with [Al] and [B]. Incidentally, the
612 same analysis performed on the LA-HSiEt₃ adducts shows that
613 the 10 kcal/mol of difference in the relative stability of the
614 [Al]...H-SiEt₃ adduct with respect to the [B]...H-SiEt₃ one
615 decreased to -2 kcal/mol in favor of the borane when AlH₃
616 and BH₃ are used as the LA. This suggests that steric effects
617 strongly impact the binding ability of [B].

As a further test, we decomposed the gas-phase binding energy of [Al] and [B] to formaldehyde into a preparation and an interaction energy term. The first contribution is the energy paid to deform the LA and the aldehyde from their ideal conformations in the unbound state to the geometries they assume in the LA-adducts E. The interaction energy term, instead, corresponds to the energy gain due to the rigid interaction between the LA and the aldehyde frozen in the same conformation as in E. We found that the deformation of the free [B] to the geometry it has in E is 9.5 kcal/mol more expensive than the deformation of [Al], while the interaction energy between the deformed LA and formaldehyde is only 6.5 kcal/mol stronger with [Al]. The two terms cumulate in an [Al]-aldehyde bond being 16.0 kcal/mol stronger than the [B]-aldehyde bond in the gas-phase.

Overall, these results indicated that the different behavior of [Al] and [B] can be ascribed to the significantly smaller size of boron that causes unfavorable steric repulsions between the C₆F₅ rings, as well as between the C₆F₅ rings and the substituents on the silane atoms, in the adducts.

In Scheme 7 we summarized the whole catalytic cycle in the presence of both [Al] and [B] LAs, while the calculated energy profiles of intermediates and transition states for [Al] and [B] pathways along the reaction coordinate were plotted in Figure 6. As the first step, hydrosilylation of CO₂ to silylformate takes place via the [Al] catalyzed C=O activation pathway. Next, the reduction of HCOOSiEt₃ to formaldehyde proceeds through the [B] catalyzed SN₂-type Si-H activation mechanism. In the following reduction step to achieve intermediate Et₃SiOCH₃, the C=O and the Si-H activation pathways turn out as competitive with [B] since the corresponding determining barriers are almost the same in energy. Finally, in the last reduction step to methane, the SN₂ Si-H activation mechanism is again favored. The sterics of the substrate seems to play a key role, with the C=O activation pathway suffering the steric hindrance more than the SN₂ Si-H one due to a more crowded geometry of the corresponding transition state.³⁷ The thermodynamics of the adducts favors [Al]; however, in agreement with the experimental results, only [Al] is active in the first step, while [B] is active in the subsequent steps. As a consequence an exchange between the two Lewis acids is likely to take place during the four reduction steps.

CONCLUSIONS

In summary, we have developed the first example of highly selective reduction of CO₂ into CH₄ via tandem catalytic hydrosilylation by a mixed main-group B(C₆F₅)₃/Al(C₆F₅)₃ catalyst system. The results, obtained from our comprehensive study involving the detection, characterization, and independent synthesis of each reaction intermediate, reactions under catalytic conditions, and computational calculations as well as kinetic and mechanistic investigations, have demonstrated that [Al] is responsible for the first step of the reduction that converts CO₂ into HCOOSiEt₃, while the subsequent reduction steps of HCOOSiEt₃ to H₂C(OSiEt₃)₂ to H₃COSiEt₃ and finally to CH₄ are catalyzed by [B]. The hydrosilylation of H₂C(OSiEt₃)₂, the rate-limiting step in the [B]-catalyzed FLP reduction sequences, is proposed to proceed through a two-step pathway involving the formation and reduction of formaldehyde. Our computational results further address the fixation of CO₂ into HCOOSiEt₃ by [Al] via the classical LA-mediated C=O activation, the subsequent transformations into CH₄ by [B] through the FLP-type Si-H activation, as well as

the H₂C(OSiEt₃)₂ reduction via the formaldehyde cycle, all of which are consistent with the experimental results.

We attribute this remarkably different catalytic behavior between Al(C₆F₅)₃ and B(C₆F₅)₃ to the higher overall Lewis acidity of [Al] derived from two conflicting factors, electronic and steric effects. While the study of the electronic term indicates that [B] has a higher electronic affinity, the steric term suggests that [B] pays much higher reorganization energy penalty due to both a smaller radius of boron and repulsion between the *ortho*-fluorine atoms. This stronger overall Lewis acidity of [Al], when compared to [B], renders its higher tendency to form stable [Al]-substrate (intermediate) adducts with CO₂ as well as intermediates 1, 2, and 3, hence accounting for its distinct yet complementary catalytic behaviors in the CO₂-to-CH₄ hydrosilylative reduction cycle. Overall, the roles of [Al] and [B] are not only complementary but also synergistic in the total reduction of CO₂, which render both [Al]-mediated first reduction step (which, when carried out alone, is a stoichiometric reaction) and [B]-mediated subsequent steps catalytic. With an optimized loading and [Al]/[B] ratio of 1.0%:5.0%, a high CH₄ production yield of 94% has been achieved. Such a catalytic system is also shown to be recyclable based on three cycling experiments. The tunability of [Al]/[B] catalysts should allow one to develop more efficient, economical, and recyclable tandem LA catalysts based on inter- or intramolecular and/or heterogeneous catalysts.

ASSOCIATED CONTENT

Supporting Information

The Supporting Information is available free of charge on the ACS Publications website at DOI: 10.1021/jacs.6b01497.

- Full experimental details, additional figures, and complete ref 36 (PDF)
- Crystallographic data (CIF)
- Crystallographic data (CIF)

AUTHOR INFORMATION

Corresponding Authors

*laura.falivene@kaust.edu.sa

*eugene.chen@colostate.edu

Notes

The authors declare no competing financial interest.

ACKNOWLEDGMENTS

This work was supported by the U.S. National Science Foundation (NSF- CHE-1507702) for the study carried out at Colorado State University and by the funding from King Abdullah University of Science and Technology (KAUST) for the study performed at KAUST. We thank Boulder Scientific Co. for the research gift of B(C₆F₅)₃.

REFERENCES

- (1) (a) *Carbon Dioxide as Chemical Feedstock*. Aresta, M., Ed.; Wiley-VCH: Weinheim, 2010. (b) Olah, G. A. *Angew. Chem., Int. Ed.* **2005**, *44*, 2636–2639.
- (2) For recent reviews of carbon dioxide conversion and reduction, see: (a) Maeda, C.; Miyazaki, Y.; Ema, T. *Catal. Sci. Technol.* **2014**, *4*, 1482–1497. (b) Oh, Y.; Hu, X. *Chem. Soc. Rev.* **2013**, *42*, 2253–2261. (c) Costentin, C.; Robert, M.; Savéant, J. M. *Chem. Soc. Rev.* **2013**, *42*, 2423–2436. (d) Centi, G.; Quadrelli, E. A.; Perathoner, S. *Energy Environ. Sci.* **2013**, *6*, 1711–1731. (e) Peters, M.; Köhler, B.; Kuckshinrichs, W.; Leitner, W.; Markewitz, P.; Müller, T. E. *ChemSusChem* **2011**, *4*, 1216–1240. (f) Cokoja, M.; Bruckmeier, C.;

- 739 Rieger, B.; Herrmann, W. A.; Kühn, F. E. *Angew. Chem., Int. Ed.* **2011**,
740 *50*, 8510–37. (g) Riduan, S. N.; Zhang, Y. *Dalton Trans.* **2010**, 39,
741 3347–3357. (h) Benson, E. E.; Kubiak, C. P.; Sathrum, A. J.; Smieja, J.
742 *M. Chem. Soc. Rev.* **2009**, 38, 89–99.
- 743 (3) For a recent review of catalytic carbon dioxide hydrosilylation,
744 see: Fernández-Alvarez, F. J.; Aitani, A. M.; Oro, L. A. *Catal. Sci.*
745 *Technol.* **2014**, 4, 611–624.
- 746 (4) For recent reviews of catalytic carbon dioxide hydrogenation, see:
747 (a) Li, Y.-N.; Ma, R.; He, L.-N.; Diao, Z.-F. *Catal. Sci. Technol.* **2014**, 4,
748 1498–1512. (b) Fernández-Alvarez, F. J.; Iglesias, M.; Oro, L. A.; Polo,
749 V. *ChemCatChem* **2013**, 5, 3481–3494. (c) Wang, W.; Wang, S.; Ma,
750 X.; Gong, J. *Chem. Soc. Rev.* **2011**, 40, 3703–3727. (d) Federsel, C.;
751 Jackstell, R.; Beller, M. *Angew. Chem., Int. Ed.* **2010**, 49, 6254–6257.
752 (e) Jessop, P. G.; Joó, F.; Tai, C.-C. *Coord. Chem. Rev.* **2004**, 248,
753 2425–2442. (f) Leitner, W. *Angew. Chem., Int. Ed. Engl.* **1995**, 34,
754 2207–2221.
- 755 (5) (a) Metsanen, T. T.; Oestreich, M. *Organometallics* **2015**, 34,
756 543–546. (b) Deglmann, P.; Ember, E.; Hofmann, P.; Pitter, S.;
757 Walter, O. *Chem. - Eur. J.* **2007**, 13, 2864–2879. (c) Jansen, A.; Görls,
758 H.; Pitter, S. *Organometallics* **2000**, 19, 135–138. (d) Süß-Fink, G.;
759 Reiner, J. *J. Organomet. Chem.* **1981**, 221, C36–C38. (e) Koinuma, H.;
760 Kawakami, F.; Kato, H.; Hirai, H. *J. Chem. Soc., Chem. Commun.* **1981**,
761 213–214.
- 762 (6) Scheuermann, M. L.; Semproni, S. P.; Pappas, I.; Chirik, P. J.
763 *Inorg. Chem.* **2014**, 53, 9463–9465.
- 764 (7) Itagaki, S.; Yamaguchi, K.; Mizuno, N. *J. Mol. Catal. A: Chem.*
765 **2013**, 366, 347–352.
- 766 (8) (a) Lalrempuia, R.; Iglesias, M.; Polo, V.; Miguel, P. J. S.;
767 Fernández-Alvarez, F. J.; Pérez-Torrente, J. J.; Oro, L. A. *Angew. Chem.,*
768 *Int. Ed.* **2012**, 51, 12824–12827. (b) Park, S.; Bézier, D.; Brookhart,
769 M. *J. Am. Chem. Soc.* **2012**, 134, 11404–11407. (c) Eisenschmid, T. C.;
770 Eisenberg, R. *Organometallics* **1989**, 8, 1822–1824.
- 771 (9) González-Sebastián, L.; Flores-Alamo, M.; García, J. J. *Organo-*
772 *metallics* **2013**, 32, 7186–7194.
- 773 (10) (a) Zhang, L.; Cheng, J. H.; Hou, Z. M. *Chem. Commun.* **2013**,
774 49, 4782–4784. (b) Motokura, K.; Kashiwame, D.; Takahashi, N.;
775 Miyaji, A.; Baba, T. *Chem. - Eur. J.* **2013**, 19, 10030–10037.
776 (c) Motokura, K.; Kashiwame, D.; Miyaji, A.; Baba, T. *Org. Lett.*
777 **2012**, 14, 2642–2645.
- 778 (11) Sattler, W.; Parkin, G. *J. Am. Chem. Soc.* **2012**, 134, 17462–
779 17465.
- 780 (12) (a) Piers, W. E. *Adv. Organomet. Chem.* **2004**, 52, 1–76.
781 (b) Chen, E. Y.-X.; Marks, T. J. *Chem. Rev.* **2000**, 100, 1391–1434.
- 782 (13) Matsuo, T.; Kawaguchi, H. *J. Am. Chem. Soc.* **2006**, 128, 12362–
783 12363.
- 784 (14) Mitton, S. J.; Turculet, L. *Chem. - Eur. J.* **2012**, 18, 15258–
785 15262.
- 786 (15) Jiang, Y. F.; Blacque, O.; Fox, T.; Berke, H. *J. Am. Chem. Soc.*
787 **2013**, 135, 7751–7760.
- 788 (16) (a) LeBlanc, F. A.; Piers, W. E.; Parvez, M. *Angew. Chem., Int.*
789 *Ed.* **2014**, 53, 789–792. (b) Berkefeld, A.; Piers, W. E.; Parvez, M.;
790 Castro, L.; Maron, L.; Eisenstein, O. *Chem. Sci.* **2013**, 4, 2152–2162.
- 791 (17) For selected reviews of the FLP chemistry, see: (a) Stephan, D.
792 W.; Erker, G. *Angew. Chem., Int. Ed.* **2015**, 54, 6400–6441.
793 (b) Stephan, D. W.; Erker, G., Eds.; *Frustrated Lewis Pairs I & II,*
794 *Topics in Current Chemistry*; Springer-Verlag: Berlin, Germany, 2013;
795 Vols. 332 & 334. (c) Stephan, D. W.; Erker, G. *Angew. Chem., Int. Ed.*
796 **2010**, 49, 46–76.
- 797 (18) Ashley, A. E.; Thompson, A. L.; O'Hare, D. *Angew. Chem., Int.*
798 *Ed.* **2009**, 48, 9839–9843.
- 799 (19) Menard, G.; Stephan, D. W. *J. Am. Chem. Soc.* **2010**, 132, 1796–
800 1797.
- 801 (20) Courtemanche, M.-A.; Légaré, M.-A.; Maron, L.; Fontaine, F.-G.
802 *J. Am. Chem. Soc.* **2013**, 135, 9326–9329.
- 803 (21) For recent reviews of carbon dioxide reduction utilizing the
804 FLP chemistry, see: (a) Bontemps, S. *Coord. Chem. Rev.* **2016**, 308,
805 117–130. (b) Fontaine, F.-G.; Courtemanche, M.-A.; Légaré, M.-A.
806 *Chem. - Eur. J.* **2014**, 20, 2990–2996.
- (22) (a) Declercq, R.; Bouhadir, G.; Bourissou, D.; Légaré, M.-A.; 807
Courtemanche, M.-A.; Nahi, K. S.; Bouchard, N.; Fontaine, F.-G.; 808
Maron, L. *ACS Catal.* **2015**, 5, 2513–2520. (b) Courtemanche, M.-A.; 809
Pulis, A. P.; Rochette, E.; Légaré, M.-A.; Stephan, D. W.; Fontaine, F.- 810
G. *Chem. Commun.* **2015**, 51, 9797–9800. (c) Wang, T.; Stephan, D. 811
W. Chem. - Eur. J. **2014**, 20, 3036–3039. (d) Gomes, C. D.; Blondiaux, 812
E.; Thuéry, P.; Cantat, T. *Chem. - Eur. J.* **2014**, 20, 7098–7106. 813
(e) Courtemanche, M.-A.; Légaré, M.-A.; Maron, L.; Fontaine, F.-G. *J.* 814
Am. Chem. Soc. **2014**, 136, 10708–10717. (f) Menard, G.; Stephan, D. 815
W. Dalton Trans. **2013**, 42, 5447–5453. (g) Lim, C. H.; Holder, A. M.; 816
Hynes, J. T.; Musgrave, C. B. *Inorg. Chem.* **2013**, 52, 10062–10066. 817
(h) Courtemanche, M.-A.; Larouche, J.; Légaré, M.-A.; Bi, W.; Maron, 818
L.; Fontaine, F.-G. *Organometallics* **2013**, 32, 6804–6811. (i) Roy, L.; 819
Zimmerman, P. M.; Paul, A. *Chem. - Eur. J.* **2011**, 17, 435–439. 820
(j) Kwon, H. J.; Kim, H. W.; Rhee, Y. M. *Chem. - Eur. J.* **2011**, 17, 821
6501–6507. (k) Zimmerman, P. M.; Zhang, Z. Y.; Musgrave, C. B. 822
Inorg. Chem. **2010**, 49, 8724–8728. 823
- (23) Riduan, S. N.; Zhang, Y. G.; Ying, J. Y. *Angew. Chem., Int. Ed.* 824
2009, 48, 3322–3325. 825
- (24) Berkefeld, A.; Piers, W. E.; Parvez, M. *J. Am. Chem. Soc.* **2010**, 826
132, 10660–10661. 827
- (25) Schäfer, A.; Saak, W.; Haase, D.; Müller, T. *Angew. Chem., Int.* 828
Ed. **2012**, 51, 2981–2984. 829
- (26) (a) Wehmschulte, R. J.; Saleh, M.; Powell, D. R. *Organometallics* 830
2013, 32, 6812–6819. (b) Khandelwal, M.; Wehmschulte, R. J. *Angew.* 831
Chem., Int. Ed. **2012**, 51, 7323–7326. 832
- (27) Chen, E. Y.-X. Tris(pentafluorophenyl)alane. In *Encyclopedia of* 833
Reagents for Organic Synthesis; John Wiley & Sons, Ltd: Hoboken, NJ, 834
2012, DOI:10.1002/047084289X.rm01382. 835
- (28) (a) Oestreich, M.; Hermeke, J.; Mohr, J. *Chem. Soc. Rev.* **2015**, 836
44, 2202–2220. (b) Houghton, A. Y.; Hurmalainen, J.; Mansikkamaki, 837
A.; Piers, W. E.; Tuononen, H. M. *Nat. Chem.* **2014**, 6, 983–988. 838
(c) Sakata, K.; Fujimoto, H. *J. Org. Chem.* **2013**, 78, 12505–12512. 839
(d) Piers, W. E.; Marwitz, A. J. V.; Mercier, L. G. *Inorg. Chem.* **2011**, 840
50, 12252–12262. (e) Rendler, S.; Oestreich, M. *Angew. Chem., Int. Ed.* 841
2008, 47, 5997–6000. (f) Chojnowski, J.; Rubinsztajn, S.; Cella, J. A.; 842
Fortuniak, W.; Cypriak, M.; Kurjata, J.; Kaźmierski, K. *Organometallics* 843
2005, 24, 6077–6084. (g) Gevorgyan, V.; Rubin, M.; Liu, J.-X.; 844
Yamamoto, Y. *J. Org. Chem.* **2001**, 66, 1672–1675. (h) Parks, D. J.; 845
Blackwell, J. M.; Piers, W. E. *J. Org. Chem.* **2000**, 65, 3090–3098. 846
(i) Gevorgyan, V.; Rubin, M.; Benson, S.; Liu, J.-X.; Yamamoto, Y. *J.* 847
Org. Chem. **2000**, 65, 6179–6186. (j) Parks, D. J.; Piers, W. E. *J. Am.* 848
Chem. Soc. **1996**, 118, 9440–9441. 849
- (29) To confirm this statement on B(C₆F₅)₃ from ref 13, we carried 850
out additional control experiments under our conditions (Table 1, 851
entries 1 and 2). For entry 2, we found no CH₄ formation and only 852
small silane consumption (~2%), presumably due to the trans- 853
metalation between Et₃SiH and B(C₆F₅)₃ in the absence of basic 854
substrates, as reported in: Parks, D. J.; Piers, W. E.; Yap, G. P. A. 855
Organometallics **1998**, 17, 5492–5503. 856
- (30) (a) Chen, J.; Chen, E. Y.-X. *Angew. Chem., Int. Ed.* **2015**, 54, 857
6842–6846. (b) Chen, J.; Chen, E. Y.-X. *Molecules* **2015**, 20, 9575– 858
9590. (c) Timoshkin, A. Y.; Frenking, G. *Organometallics* **2008**, 27, 859
371–380. (d) Rodriguez-Delgado, A.; Chen, E. Y.-X. *J. Am. Chem. Soc.* 860
2005, 127, 961–974. (e) Feng, S.; Roof, G. R.; Chen, E. Y.-X. 861
Organometallics **2002**, 21, 832–839. (f) Chen, E. Y.-X.; Kruper, W. J.; 862
Roof, G.; Wilson, D. R. *J. Am. Chem. Soc.* **2001**, 123, 745–746. 863
- (31) Chen, J.; Chen, E. Y.-X. *Dalton Trans.* **2016**, 45, 6105. 864
- (32) Hair, G. S.; Cowley, A. H.; Jones, R. A.; McBurnett, B. G.; Voigt, 865
A. J. Am. Chem. Soc. **1999**, 121, 4922–4923. 866
- (33) Ménard, G.; Gilbert, T. M.; Hatnean, J. A.; Kraft, A.; Crossing, 867
I.; Stephan, D. W. *Organometallics* **2013**, 32, 4416–4422. 868
- (34) Großekappenberg, H.; Lühmann, N.; Saak, W.; Müller, T. Z. 869
Anorg. Allg. Chem. **2015**, 641, 2543–2548. 870
- (35) Huang, F.; Lu, G.; Zhao, L. L.; Li, H. X.; Wang, Z.-X. *J. Am.* 871
Chem. Soc. **2010**, 132, 12388–12396. 872
- (36) DFT static calculations were performed using the Gaussian 09 873
package, see the SI for full computational details. 874

875 (37) This result is in agreement with the observations reported in ref
876 28c for the hydrosilylation of acetone with Me_3SiH and $\text{B}(\text{C}_6\text{F}_5)_3$. In
877 fact, comparing the barrier for the reduction of acetone with that for
878 the reduction of the less hindered formaldehyde, the $\text{C}=\text{O}$ pathway
879 turns out to be much unfavored for the ketone substrate.